Article

Electrolyte Optimization to Improve the High-Voltage Operation of Single-Crystal LiNi$_{0.83}$Co$_{0.11}$Mn$_{0.06}$O$_2$ in Lithium-Ion Batteries

Wengao Zhao [1,2,*,†], Mayan Si [1,3,†], Kuan Wang [4,†], Enzo Brack [1], Ziyan Zhang [2], Xinming Fan [5,*] and Corsin Battaglia [1,3]

[1] Materials for Energy Conversion Laboratory, Swiss Federal Laboratories for Materials Science and Technology (EMPA), 8600 Dubendorf, Switzerland; simayansmy@gmail.com (M.S.); enzobrack@bluewin.ch (E.B.); cosin.battaglia@empa.ch (C.B.)
[2] Institute of Nanotechnology, Karlsruhe Institute of Technology, 76344 Eggenstein-Leopoldshafen, Germany; ziyanzhang0116@gmail.com
[3] Department of Materials, Eidgenossische Technische Hochschule (ETH) Zurich, 8093 Zurich, Switzerland
[4] GRINM (Guangdong) Institute for Advanced Materials and Technology Foshan, Foshan 528051, China; wangkuan1991@163.com
[5] School of Metallurgy and Environment, Central South University, Changsha 410083, China
* Correspondence: wengao.zhao@kit.edu (W.Z.); fanxm@csu.edu.cn (X.F.)
† These authors contributed equally to this work.

Abstract: Single-crystal Ni-rich layered oxide materials LiNi$_{1-x-y}$Co$_x$Mn$_y$O$_2$ (NCM, $1 - x - y \geq 0.6$) are emerging as promising cathode materials that do not show intergranular cracks as a result of the lack of grain boundaries and anisotropy of the bulk structure, enabling extended cyclability in lithium-ion batteries (LIBs) operating at high voltage. However, SC-NCM materials still suffer from capacity fading upon extended cycling. This degradation of capacity can be attributed to a reconstruction of the surface. A phase transformation from layered structures to disordered spinel/rock-salt structures was found to be responsible for impedance growth and capacity loss. Film-forming additives are a straightforward approach for the mitigation of surface reconstruction via the formation of a robust protection layer at the cathode's surface. In this work, we investigate various additives on the electrochemical performance of single-crystal LiNi$_{0.83}$Co$_{0.11}$Mn$_{0.06}$O$_2$ (SC-NCM83). The results demonstrate that the use of 1% lithium difluoroxalate borate (LiDFOB) and 1% lithium difluorophosphate (LiPO$_2$F$_2$) additives substantially enhanced the cycling performance (with a capacity retention of 93.6% after 150 cycles) and rate capability in comparison to the baseline electrolyte (72.7%) as well as electrolytes using 1% LiDFOB (90.5%) or 1% LiPO$_2$F$_2$ (88.3%) individually. The superior cycling stability of the cell using the combination of both additives was attributed to the formation of a conformal cathode/electrolyte interface (CEI) layer, resulting in a stabilized bulk structure and decreased impedance upon long-term cycling, as evidenced via a combination of state-of-the-art analytical techniques.

Keywords: high-voltage operation; enhanced cycling performance; decreased impedance; conformal cathode/electrolyte interface layer

1. Introduction

The first commercialization of LIBs was realized by Sony Corporation in 1991 [1]. Over the past three decades, LIBs have been widely used in portable electronics and electric vehicles due to their high energy density. Ni-rich layered oxide materials, LiNi$_{1-x-y}$Co$_x$Mn$_y$O$_2$ (NCM, $1 - x - y \geq 0.6$), have been identified as one of the most promising cathode materials as a result of the synergistic effects of transition metals, such as their high specific capacity, high operating voltage, adequate rate capability, and reasonable cost [2]. Conventional polycrystalline NCM cathode materials consist of hundreds of nanometer-sized

primary particles containing internal grain boundaries. These materials are prone to form intergranular cracks initiated along the grain boundaries during extended battery operations [3], due to anisotropic volume changes during lithium insertion and extraction [4]. Intergranular cracks may propagate from the particle's bulk structure to its surfaces, especially during high-voltage operation or long-term cycling, ultimately leading to structural collapse [4]. The cracks effectively increase the electrode/electrolyte interface area, exacerbating surface-related degradations such as surface reconstruction, transition metal dissolution, and oxygen release [3], consequentially resulting in capacity loss.

Previous research suggested that single-crystalline NCM (SC-NCM) materials could address the issues of intergranular cracks whilst maintaining structural integrity by eliminating grain boundaries within the particles [4]. Qian et al. reported that SC-NCM622 exhibits a remarkable capacity retention of 94% after 300 cycles at 4.3 V operation, surpassing its polycrystalline counterpart (52%), as a consequence of the lack of intergranular cracks [3]. Similarly, Fan et al. observed that $SC-LiNi_{0.83}Co_{0.11}Mn_{0.06}O_2$ (SC-NCM83) outperforms its polycrystalline counterpart in terms of cycling performance at both 25 °C and 55 °C [4]. Furthermore, the morphology of SC-NCM83 particles remains mechanically intact, without any occurrence of cracks even after 600 cycles. This underscores the potential advantages of using SC-NCM over PC-NCM materials in LIB applications. Although SC-NCM83 efficiently removes intergranular cracks, they remain susceptible to surface layer reconstruction from a layered structure to spinel and/or rock-salt-like structures, a phenomenon that is known to worsen with increasing Ni content [5,6]. These structural changes lead to lower Li-ion conductivity, affecting lithiation and delithiation processes, which in turn result in impedance growth and capacity loss [5,6]. During the lithiation/delithation process, transition metals, especially Ni, may migrate to vacant Li sites due to the similar radii of Ni^{2+} and Li^+ ions. This migration reduces Ni to lower valence states and its dissolution into the electrolyte [6]. The reduction of Ni is typically accompanied by oxygen loss [7]. Depending on the extent of Li loss, Ni migration, and oxygen loss, both spinel and rock-salt-like structures form on the surface of the cathode particles, degrading the capacity of the cells.

To improve the surface stability of NCM materials, several strategies have been proposed, including the formation of stable coating layers [8,9] and doping with cations or anions [10,11]. An alternative strategy involves the use of film-forming electrolyte additives to build a surface protective layer to suppress parasitic reactions on the cathode/electrolyte interface. Various additives have been explored to enhance the electrochemical performance of NCM cathodes, including lithium salt-type additives such as lithium difluoroxalate borate (LiDFOB) [12] and lithium difluorophosphate ($LiPO_2F_2$) [13], as well as boron-containing additives such as tributyl borate (TBB) [14] and tris(2-cyanoethyl) borate (TCEB) [15], and phosphorous-containing additives such as triphenylphosphine oxide (TPPO) [16] and 2-(2,2,2-trifluoromethoxy)-1,3,2-dioxaphospholane 2-oxide (TFEOP) [17]. Dong et al. reported that the addition of 1.5% LiDFOB into a carbonate-based electrolyte (1 M $LiPF_6$ in ethylene carbonate (EC)/dimethyl carbonate (DMC)/ethyl methyl carbonate (EMC) (1:1:1, *v:v:v*)) significantly improved the cycling stability of graphite‖$LiNi_{0.83}Mn_{0.05}Co_{0.12}O_2$ cells from 59.9% to 83.1% capacity retention after 200 cycles in the voltage range 2.8–4.3 V [18]. X-ray photoelectron spectroscopy (XPS) analysis confirmed the formation of a stable CEI layer rich in boron and fluorine species, whilst avoiding the decomposition of $LiPF_6$ and organic electrolyte components. Shkrob et al. disclosed that the oxidation of $DFOB^-$ ions generates difluoroborane dimers, which form strong B−O bonds and an oxide surface, effectively passivating the surface and preventing electrolyte oxidation [19]. Wan et al. confirmed that LiDFOB inhibited oxygen vacancy generation by building strong B-O bonds, effectively suppressing TM migration and surface reconstruction, thus resulting in improved cycling performance [7]. $LiPO_2F_2$ was identified as another promising additive used to decrease interfacial impedance and suppress electrolyte decomposition via the formation of a stable CEI layer. Zhao et al. reported that the addition of 1 wt% $LiPO_2F_2$ to a baseline electrolyte (1 M $LiClO_4$ in EC/EMC (3:7 wt%) enhanced the cycling stability of

$Li||LiNi_{0.5}Mn_{0.25}Co_{0.25}O_2$ cells, achieving 95.3% capacity retention after 100 cycles in the voltage range of 3.0–4.3 V, superior to 40.8% of cells when using the baseline electrolyte [13]. They ascribed the improved cyclability to the decreased cell impedance and suppressed electrolyte decomposition because of the compact CEI layer. Li et al. showed that the incorporation of 1% $LiPO_2F_2$ in a baseline electrolyte (1 M $LiPF_6$ in EC/EMC (3:7 wt%)) resulted in a capacity retention of 98.3% after 150 cycles in the voltage range of 2.8–4.45 V, superior to the 86.2% of the cell using the baseline electrolyte [20]. The enhanced performance was attributed to the dense, stable LiF-rich CEI layer.

In practical applications of LIBs, single additives may not always fulfill the requirements; thus, we need to combine additives to harness potential synergistic effects [21,22]. While LiDFOB and $LiPO_2F_2$ additives have been individually investigated, possible synergistic effects resulting from their combination remain unclear. In this study, the performance of $LiNi_{0.83}Co_{0.11}Mn_{0.06}O_2$ (SC-NCM83) in a carbonate-based electrolyte (1M $LiPF_6$ in EC/DMC) with 1% LiDFOB and 1% $LiPO_2F_2$, as well as with both 1% LiDFOB + 1% $LiPO_2F_2$, was investigated. We reveal that cells containing both LiDFOB and $LiPO_2F_2$ additives exhibit superior cycling stability and rate performance compared to cells containing the baseline electrolyte or combined with a single additive, suggesting synergistic effects between LiDFOB and $LiPO_2F_2$. The underlying mechanism was examined via electrochemical impedance spectroscopy (EIS), X-ray photoelectron spectroscopy (XPS), and transmission electron microscopy (TEM). The results indicate that a combination of LiDFOB and $LiPO_2F_2$ additives efficiently suppresses impedance growth whilst maintaining bulk structural integrity, thus inhibiting electrolyte decomposition upon cycling via the formation of a robust and conformal CEI layer.

2. Materials and Methods

2.1. Materials

The synthesis followed a methodology previously reported in the literature [4]. The $Ni_{0.83}Co_{0.11}Mn_{0.06}(OH)_2$ precursor was prepared via a co-precipitation method. Aqueous solutions (2M) of $NiSO_4·6H_2O$, $CoSO_4·7H_2O$, and $MnSO_4·5H_2O$, with a molar ratio of Ni:Co:Mn of 83:11:06, were simultaneously introduced into a continuously stirred tank reactor under a nitrogen atmosphere. Subsequently, appropriate amounts of NaOH solutions (5M) and $NH_3·H_2O$ solutions (4M) were fed separately to the reactor in order to adjust the pH (11.5) whilst stirring (500 rpm) at a temperature of 50 °C. The co-precipitated $Ni_{0.83}Co_{0.11}Mn_{0.06}(OH)_2$ particles were subsequently washed, filtered, and dried in a vacuum oven at 110 °C. Next, the precursor was mixed with $LiOH·H_2O$ at a Li:TM ratio of 1.06:1 and annealed at 500 °C for 5 h, followed by calcination at 830 °C for 10 h in an oxygen atmosphere to obtain the SC-NCM83 particles.

2.2. Characterizations

XRD was employed to investigate the crystalline structure of SC-NCM83 particles. The Bragg angle (2θ) was scanned from 10°–90° at a rate of 1°/min. Scanning Electron Microscopy (SEM, Manufacturer: FEI, Hillsboro, OR, USA) was used to examine the morphology and microstructure of the SC-NCM83 particles. The CEI composition of cycled NMC811 cathodes was analyzed using XPS on a PHI Quantum 2000 (Manufacturer: Physical Electronics, Chanhassen, MN, USA) with a pass energy of 30 eV. The surface structure of the cycled cathode was performed on transmission electron microscopy (TEM, 2100F, JEOL). TEM samples were prepared by FIB (FEI Helios DualBeam, Manufacturer: ThermoFisher, Waltham, MA, USA). The HAADF-STEM imaging was performed on an JEOL ARM 200CF (Manufacturer: JEOL, Tokyo, Japan) with an operation voltage of 200 kV. Before any characterization, the cycled cathodes, harvested from fully discharged cells after cycling, were washed 3 times in DMC solvent to remove residual salts.

2.3. Electrochemical Measurement

To prepare the cathode, a homogeneous slurry was formed by mixing 90 wt% SC-NCM83, 5 wt% carbon black, and 5 wt% polyvinylidene fluoride (PVDF) in N-Methyl-2-pyrrolidone (NMP). The slurry was subsequently coated onto an aluminum current collector and dried for 12 h under vacuum conditions at 100 °C. Additionally, 2032-type coin cells were assembled in an argon-filled glovebox with Li metal as the anode and polypropylene as the separator. 1M $LiPF_6$ in EC/DMC (3:7 wt%) was chosen as the baseline electrolyte whilst exploring the addition of different additives, namely 1% wt LiDFOB, 1% wt $LiPO_2F_2$, and a combination of 1% wt LiDFOB + 1% wt $LiPO_2F_2$. The mass loadings of the active cathode materials were in the range of 5.4–9.2 mg cm^{-2}.

Galvanostatic charge/discharge tests were conducted at room temperature within a 2.7–4.4 V voltage range using a BioLogic electrochemical workstation. For the cycling test, all coin cells underwent two initial formation cycles at 0.1 C/0.1 C rate, followed by 0.2 C charging/0.5 C discharging rate (1 C = 200 mA g^{-1}). EIS was employed to investigate the impedance variation of the cells after charging to 4.3 V after the 1st, 10th, 50th, and 100th cycles. EIS measurements used the potentiostatic mode with a sinusoidal amplitude of 10 mV and a frequency range from 10 mHz to 10 kHz.

3. Results and Discussions

The SC-NCM83 cathode was synthesized by co-precipitation and subsequent calcination at 830 °C in an O_2 atmosphere (see Experimental section for details). SEM images at different magnifications of the SC-NCM83 particles are shown in Figure 1a,b, indicating an average particle with a size of 2–3 µm. In Figure 1c, the X-ray diffraction (XRD) pattern displays a higher degree of (003)/(104) facet intensity ratio along with apparent splitting of the (006)/(102) and (018)/(110) reflections, indicating a well-ordered layered structure. From Rietveld refinement, the lattice parameters are extracted and shown in Table 1. It is clear that the 2.42% intermixing of Li$^+$ and Ni^{2+} in the structure (Ni$_{Li}$ defects) further suggests well-ordered layered structure formation in SC-NCM83. The HAADF-STEM image in Figure 1d confirms the lack of internal porosity, which would benefit the bulk structural stability of the particles in long-term cycling. The highly ordered SC-NCM83 cathode material is corroborated from selected area in Figure 1d by high-resolution HAADF-STEM imaging (Figure 1e) and the corresponding fast Fourier transform (SAED, Figure 1f).

Figure 2a,b shows the cycling performance of cells using baseline electrolytes and baseline electrolytes with different additives. The coulombic efficiency exhibits a similar trend in all cases, as demonstrated in Figure 1a. All cells deliver similar initial specific capacity, while cells using additives show visibly improved cyclability compared to cells using only the baseline electrolyte. The cell using a combination of LiDFOB + $LiPO_2F_2$ additives shows the best performance, exhibiting 93.7% capacity retention after 150 cycles, in contrast to the cell using a baseline electrolyte, which retains only 72.7% of its initial capacity after 144 cycles. The cell with LiDFOB additives shows 90.5% capacity retention after 150 cycles, while the cell with $LiPO_2F_2$ additives shows only 88.3%. The cells containing additives show slightly lower initial discharge capacities but more stable cyclability compared with the cells using only the baseline electrolyte. The pronounced stability of cells containing additives may be attributed to the fact that the additives are preferentially oxidized to form a stable CEI layer along with the consumption of some active Li$^+$, thus effectively improving the electrode/electrolyte interphase stability. In Figure 2b, the cell using baseline electrolyte displays inferior cycling stability compared to the cells using additives. Figure 2c shows a comparison of the rate capabilities of the investigated cells. All cells deliver similar specific capacity at current densities below 5C (1C = 200 mA g^{-1}) rates. However, as the current density increases, specifically at a rate of 5C, the cells using baseline electrolyte and $LiPO_2F_2$ additives exhibit an abrupt drop in capacity, while the cells using a combination of LiDFOB + $LiPO_2F_2$ additives or LiDFOB additives still maintain a comparable capacity. This suggests that the combination of LiDFOB + $LiPO_2F_2$ additives improves the Li-ion

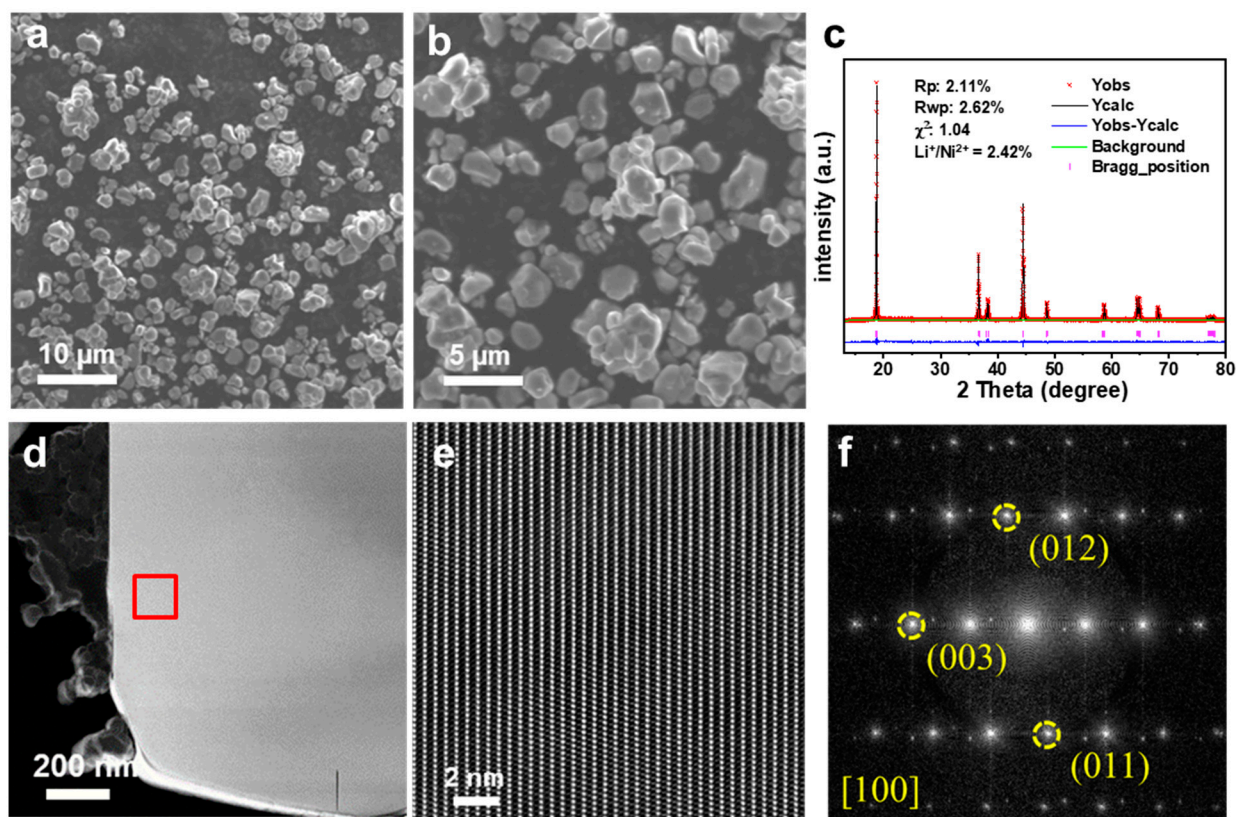transport kinetics on the electrode surface, thus enabling better performances at high rates, e.g., at 5C.

Figure 1. (**a**,**b**) SEM images, (**c**) XRD pattern and Rietveld refinement profile, (**d**) representative cross-sectional (HAADF)-(STEM) image, (**e**) high-magnification HAADF-STEM image, and (**f**) FFT pattern of the SC-NCM83.

Table 1. Lattice parameters of the SC-NCM83 cathode from Rietveld refinement analysis of XRD data.

	a (Å)	b (Å)	c (Å)	c/a	Vol(Å^3)	Ni in Li Layer (%)
SC-NCM83	2.875 (3)	2.875 (3)	14.187 (3)	4.934 (1)	101.580	2.42

To confirm the underlying reason leading to different cycling performances, the evolution of the cell's charge-discharge profiles upon cycling was examined, as shown in Figure 3. All cells show a similar Coulombic efficiency of around 87% in the first cycle, as shown in Table 2. This indicates that irreversible reactions occur during the initial charging process, which may be attributed to the electrolyte's involvement in the formation of a solid electrolyte interphase (SEI) and a CEI layer. The cells with additives show slightly lower Coulombic efficiencies in the 1st cycle, which may be attributed to the participation of the additives in the formation of SEI and CEI layers. Upon cycling, the cell using baseline shows rapid discharge voltage decay, indicating significant polarization as a result of the degradation of the interface. In sharp contrast, cells with additives—particularly those with LiDFOB + LiPO$_2$F$_2$—show considerably less voltage decay, suggesting a stable electrode/electrolyte interface contributing less pronounced polarization and, thus, higher capacity retention.
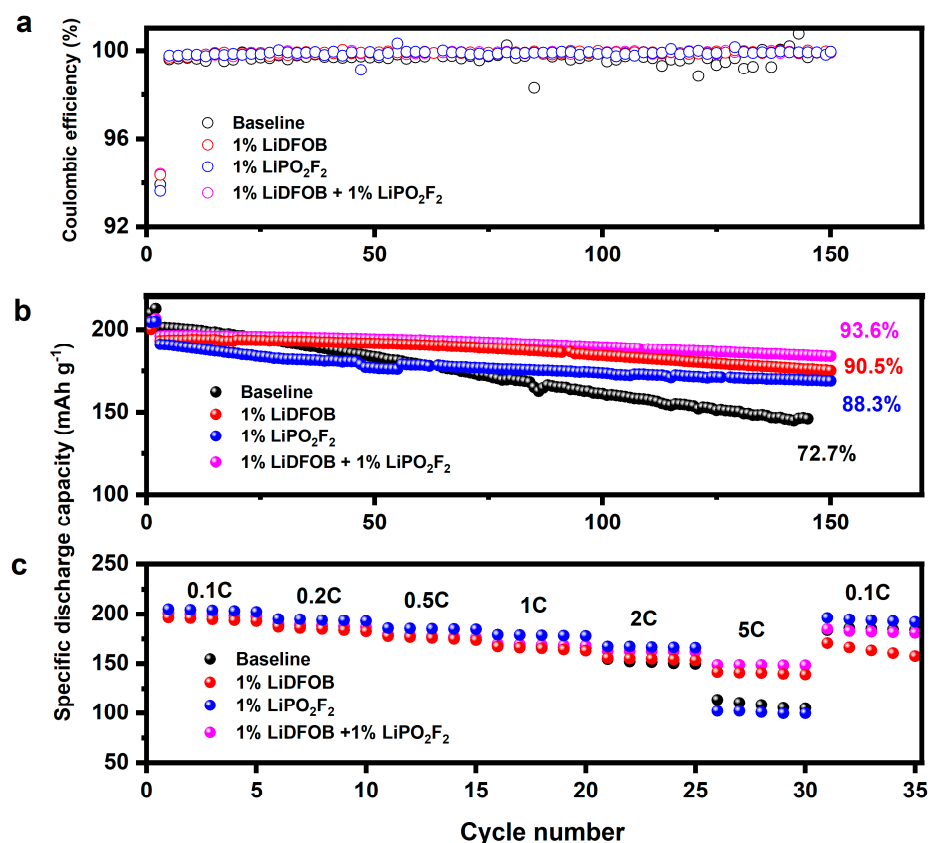
Figure 2. Electrochemical performance of Li | | SC-NCM83 cells in baseline electrolyte and upon addition of different additives. (**a**) Specific discharge capacity, (**b**) Coulombic efficiency, and (**c**) Rate performance.
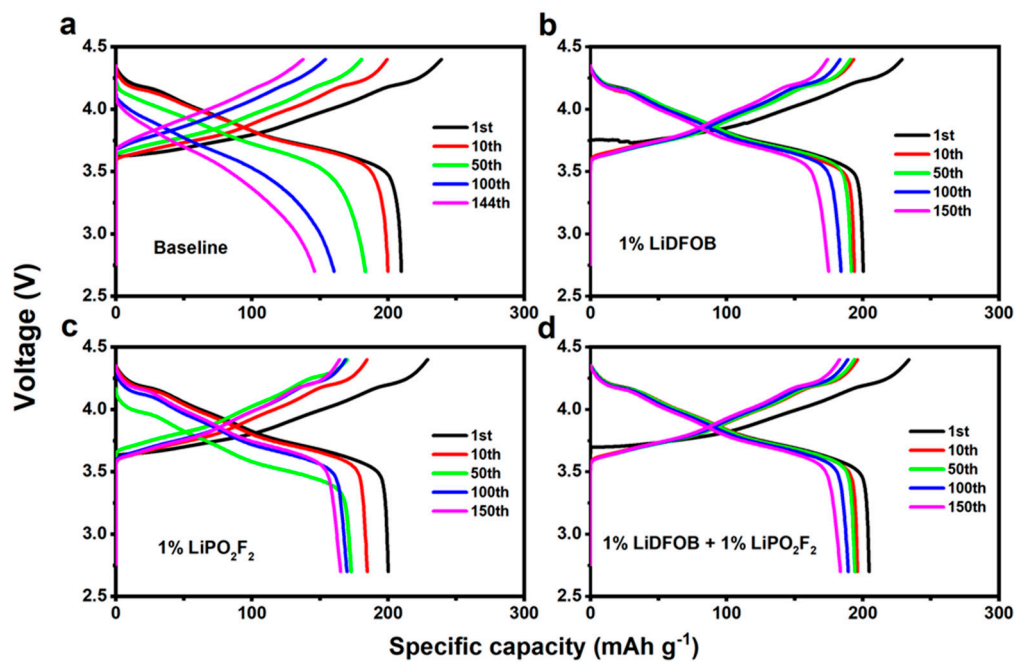

Figure 3. Charge-discharge profile evolution of Li | | SC-NCM83 cells in baseline electrolyte and upon addition of several additives. (**a**) Baseline, (**b**) LiDFOB, (**c**) $LiPO_2F_2$, (**d**) LiDFOB + $LiPO_2F_2$.

Table 2. Coulombic efficiency of the cells using baseline and different additives.

	Coulombic Efficiency (%)			
Electrolyte	Baseline	1% LiDFOB + 1% LiPO$_2$F$_2$	1% LiDFOB	1% LiPO$_2$F$_2$
1st cycle	87.7	87.5	87.6	87.4

To elucidate the origin of the improved cycling stability and rate performance of the cells using additives, EIS measurements were conducted after a specific number of cycles, as shown in Figure 4. The Nyquist plots exhibit two semicircles and a tail. The semicircle in the high-mid frequency range represents surface film resistances (R$_{sf}$) during the charging/discharging of the electrochemical double layer, while the semicircle in the mid-low frequency range corresponds to the charge-transfer resistances (R$_{ct}$) [23]. The tail at low frequencies can be attributed to Li$^+$ diffusion into the bulk electrode material. A corresponding circuit is shown in Figure 4c, where R$_b$ signifies the equivalent series resistance, CPE1 and CPE2 denote constant phase elements to model the non-ideal capacitive behavior in the electrode, and Wo1 represents the Warburg element, accounting for Li$^+$ diffusion in the low-frequency range. Fitting results for R$_{sf}$ and R$_{ct}$ are summarized in Table 3. The cell using baseline electrolyte shows large R$_{sf}$ and R$_{ct}$, which further increase upon cycling. The growth of R$_{ct}$ is particularly noticeable, as it jumps from 22 Ω at the 10th cycle to 255 Ω at the 100th cycle. This rise in resistance may be attributed to the accumulation of a poorly conductive surface film on the electrode/electrolyte interface [24,25]. Compared to the cell using baseline electrolyte, the cell using LiDFOB or LiPO$_2$F$_2$ additives individually delivers reduced R$_{ct}$, although showing comparable R$_{sf}$. Thus, the overall impedance is decreased when utilizing LiDFOB or LiPO$_2$F$_2$ additives individually as additives. The cell using a combination of LiDFOB + LiPO$_2$F$_2$ additives shows significantly decreased R$_{sf}$ and R$_{ct}$, as well as a suppressed increase upon cycling with respect to the other cells. These observations suggest that a combination of LiDFOB + LiPO$_2$F$_2$ additives contributes to the formation of a stable and conductive CEI layer, which accounts for the improved cycling performance and rate capability.
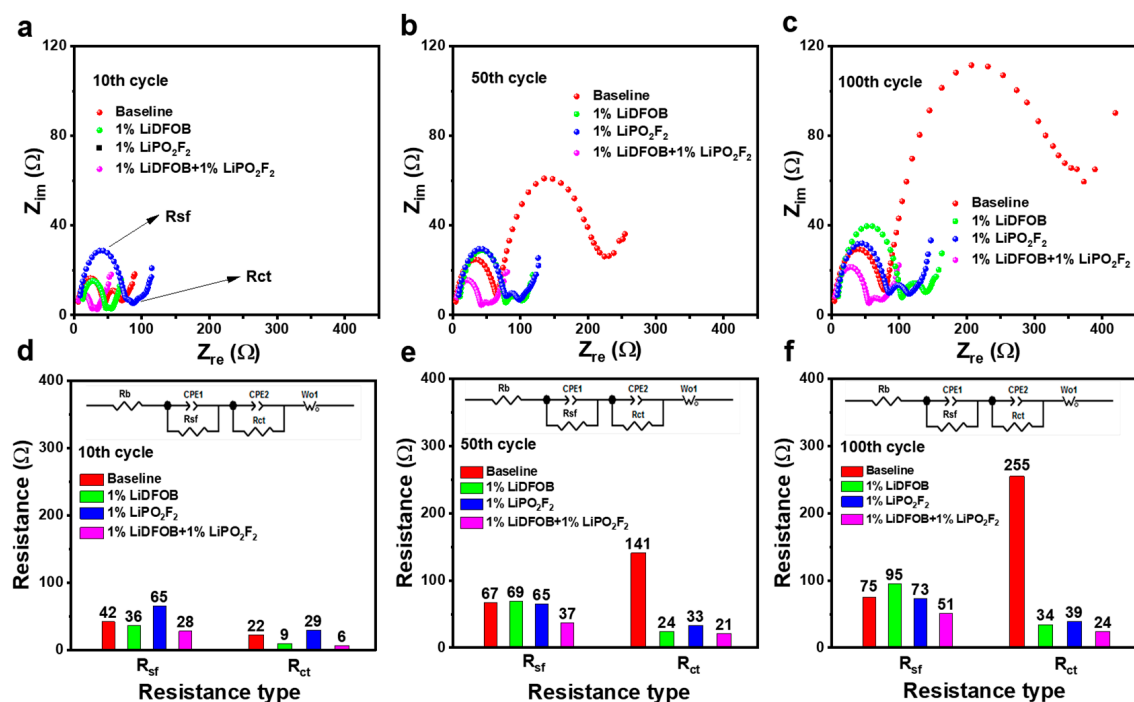

Figure 4. EIS measurements and fitting results of Li‖SC-NCM83 cells in baseline electrolytes and upon addition of additives after (**a**,**d**) 10 cycles, (**b**,**e**) 50 cycles, and (**c**,**f**) 100 cycles.

Table 3. R_{sf} and R_{ct} of the cells using different electrolytes after a certain cycle number extracted from EIS measurements.

Cycle	10th		50th		100th	
Impedance	R_{sf} (Ω)	R_{ct} (Ω)	R_{sf} (Ω)	R_{ct} (Ω)	R_{sf} (Ω)	R_{ct} (Ω)
Baseline	42	22	67	141	75	255
LiDFOB	36	9	69	24	95	34
LiPO$_2$F$_2$	65	29	65	33	73	39
LiDFOB + LiPO$_2$F$_2$	28	6	37	21	51	24

To understand the underlying mechanism of improved cycling performance of the SC-NCM83 cathode upon addition of additives, XPS measurements were performed and fitted to study the CEI layer composition on the cycled electrodes, as shown in Figure 5. The C 1s spectra of all cycled cathodes show characteristic peaks of C-C (284.8 eV), C-H (285.5 eV), C-O (286.7 eV), C=O (287.9 eV), and Li$_2$CO$_3$ (291.1 eV). The C-C and C-H species primarily originate from the conductive carbon (carbon black) and PVDF binder, while the C-O, C=O, and Li$_2$CO$_3$ species can be ascribed to electrolyte decomposition. Compared to the material cycled in the baseline electrolyte, cathode cycled in the electrolyte containing additives, particularly the combination of LiDFOB + LiPO$_2$F$_2$, shows much less intense C-O, C=O, and Li$_2$CO$_3$ signals, indicating a mitigation of the electrolyte decomposition. In all cases, O 1s spectra show the occurrence of species containing M-O (529.2 eV, M=Ni, Co, Mn), B-O (531.6 eV), C=O (532.2 eV), C-O (533.3 eV), and Li$_x$PO$_y$F$_z$ (534.4 eV) on the cycled electrode. The B-O peak is only present in the cells containing LiDFOB as an additive. The cycled cathode with the electrolyte containing a combination of LiDFOB + LiPO$_2$F$_2$ additives shows intense B-O and weak Li$_x$PO$_y$F$_z$ signals, indicating the formation of B-enriched CEI and the suppression of solvent decomposition. From a comparison of the F 1s spectra, the cycled cathode using additives shows the suppression of LiF (685 eV) and Li$_x$PO$_y$F$_z$ (686.8 eV) signals compared to the cathode cycled in the baseline electrolyte. The formation of highly resistive LiF results in sluggish Li$^+$ transport kinetics, ultimately resulting in capacity fading [26,27]. The C-F species (688.0 eV) originates from the PVDF binder, while the higher intensity indicates a smaller amount of decomposed electrolyte covering the cycled electrodes. The P 2p spectra exhibit characteristic peaks of P-O/P=O (134.3 eV) and Li$_x$PO$_y$F$_z$ (136.4 eV) in all cells. However, the amount of Li$_x$PO$_y$F$_z$ is substantially reduced when using a combination of LiDFOB + LiPO$_2$F$_2$ additives, further validating the suppression of LiPF$_6$ decomposition. B 1s spectra show that a considerable amount of B-O (191.6 eV) and Li-B-O (192.9 eV) species are formed on the cycled cathode surface, consistent with observations at the O 1s edge.

The possible impact of electrolyte additives on the CEI layer formation after 150 cycles was studied via high-resolution TEM to track changes in the surface morphology of the cycled cathodes. Figure 6 shows TEM images of the pristine and cycled SC-NCM83 particles in different electrolyte compositions. In Figure 6a,b, the pristine electrode shows a smooth surface, indicating no Li residual species formed during storage in a dry environment. The particles cycled in baseline electrolyte do not show any visible CEI layer, as judged from low (Figure 6c) as well as highly magnified (Figure 6d) high-resolution TEM images. As a consequence, surface corrosion is observed in Figure 6d, which is known to be one of the reasons responsible for the performance degradation in terms of cycling stability [12]. Thus, we were able to confirm the absence of CEI layer formation on the cycled NCM cathode particle in carbonate-based electrolytes via cryogenic electron microscopy to preserve the native state [28]. This finding helps to explain why a well-wrapped CEI layer is absent on the cycled cathode surface despite intense oxidative reactions occurring at the interface. In sharp contrast, the surface of the cycled particles exhibits a visible CEI layer with a thickness of approximately 10–30 nm, which is beneficial in maintaining an intact structure of the SC-NCM83 cathode particles by preventing corrosion as a result of contact with the

acidic electrolyte. The particles cycled in the electrolyte containing LiDFOB or LiPO$_2$F$_2$ additives individually exhibit an inhomogeneous formation of a CEI layer (Figure 6e,g). This inhomogeneous thickness of the CEI layer is rationalized to hinder Li-ion transfer during battery operation, thus causing sluggish Li-ion transfer kinetics and resulting in high impedance. On the other hand, electrodes cycled in the electrolyte containing a combination of 1% LiDFOB + 1% LiPO$_2$F$_2$ additives, the formation of a mostly uniform CEI layer with a homogeneous thickness of ~10 nm, can account for the measured suppressed impedance increase, enhanced cycling stability, and superior rate performance compared to cells using single or no additives.

Figure 5. The C 1s (**a**), O 1s (**b**), F 1s (**c**), P 2p (**d**), and B 1s (**e**) spectra of the SC-NCM83 cathodes cycled in the baseline electrolyte and upon addition of additives after 150 cycles.
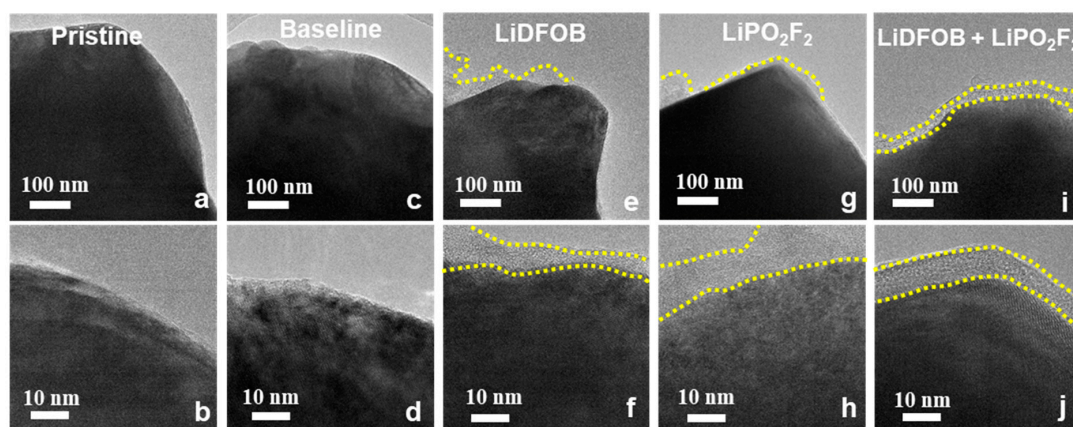

Figure 6. Representative high-resolution TEM images of the border of (**a**,**b**) pristine cathode particles. CEI layer of SC-NCM83 cathodes cycled in (**c**,**d**) baseline, (**e**,**f**) baseline + LiDFOB, (**g**,**h**) baseline + LiPO$_2$F$_2$, and (**i**,**j**) baseline + LiDFOB + LiPO$_2$F$_2$ electrolyte solutions after 150 cycles. The yellow dotted line indicates the morphology of CEI layer on the cycled cathodes.

4. Conclusions

The Li||SC-NCM83 cells using an electrolyte containing a combination of 1% LiDFOB + 1% LiPO$_2$F$_2$ additives significantly improve capacity retention (93.7% after 150 cycles) and rate performance at 4.4 V operation, superior to the electrolyte without or with the individual use of additives. The improvement is attributed to a less-pronounced formation of LiF and B-enriched protective CEI layers on the surface of cycled SC-NCM83, as it suppresses charge transfer impedance (R$_{ct}$) growth and prevents cathode corrosion that is induced by the electrolyte decomposition. A more uniform and compact CEI layer of ~10 nm was found to form on cathode particles being cycled in the electrolyte containing a combination of LiDFOB + LiPO$_2$F$_2$ additives. Additionally, the formation of a robust and conductive CEI layer was found to be helpful to maintain faster Li-ion transfer kinetics and to achieve a good rate capability. Moreover, it alleviates the continuous decomposition of the baseline electrolyte at the particle interface via the formation of a protective layer, thus maintaining an intact and stable bulk structure of the SC-NCM83 particles. To summarize, we can safely claim that the use of a combination of LiDFOB + LiPO$_2$F$_2$ additives is a promising strategy to improve the overall performance of Ni-rich SC-NCM cathode LIBs. Thus, it may be worth putting more effort into the optimization of the combination of electrolytes in order to boost the cycling stability and rate capability at high-voltage operation of Ni-rich SC-NCM via the in-situ formation of a passivating CEI layer whilst maintaining Li$^+$ diffusion properties and bulk structural integrity.

Data Availability Statement: No new data were created or analyzed in this study. Data sharing is not applicable to this article.

Conflicts of Interest: The authors declare that they have no known competing financial interests or personal relationships that could have appeared to influence the work reported in this paper.

References

1. Friedrich, F.; Strehle, B.; Freiberg, A.T.S.; Kleiner, K.; Day, S.J.; Erk, C.; Piana, M.; Gasteiger, H.A. Editors' Choice—Capacity Fading Mechanisms of NCM-811 Cathodes in Lithium-Ion Batteries Studied by X-ray Diffraction and Other Diagnostics. *J. Electrochem. Soc.* **2019**, *166*, A3760–A3774. [CrossRef]
2. Wu, Q.; Mao, S.; Wang, Z.; Tong, Y.; Lu, Y. Improving LiNi$_x$Co$_y$Mn$_{1-x-y}$O$_2$ Cathode Electrolyte Interface under High Voltage in Lithium Ion Batteries. *Nano Select* **2020**, *1*, 111–134. [CrossRef]
3. Qian, G.; Zhang, Y.; Li, L.; Zhang, R.; Xu, J.; Cheng, Z.; Xie, S.; Wang, H.; Rao, Q.; He, Y.; et al. Single-Crystal Nickel-Rich Layered-Oxide Battery Cathode Materials: Synthesis, Electrochemistry, and Intra-Granular Fracture. *Energy Storage Mater.* **2020**, *27*, 140–149. [CrossRef]
4. Fan, X.; Hu, G.; Zhang, B.; Ou, X.; Zhang, J.; Zhao, W.; Jia, H.; Zou, L.; Li, P.; Yang, Y. Crack-Free Single-Crystalline Ni-Rich Layered NCM Cathode Enable Superior Cycling Performance of Lithium-Ion Batteries. *Nano Energy* **2020**, *70*, 104450. [CrossRef]
5. Xu, C.; Märker, K.; Lee, J.; Mahadevegowda, A.; Reeves, P.J.; Day, S.J.; Groh, M.F.; Emge, S.P.; Ducati, C.; Layla Mehdi, B.; et al. Bulk Fatigue Induced by Surface Reconstruction in Layered Ni-Rich Cathodes for Li-Ion Batteries. *Nat. Mater.* **2021**, *20*, 84–92. [CrossRef] [PubMed]
6. Zhu, J.; Sharifi-Asl, S.; Garcia, J.C.; Iddir, H.H.; Croy, J.R.; Shahbazian-Yassar, R.; Chen, G. Atomic-Level Understanding of Surface Reconstruction Based on Li[Ni$_x$Mn$_y$Co$_{1-x-y}$]O$_2$ Single-Crystal Studies. *ACS Appl. Energy Mater.* **2020**, *3*, 4799–4811. [CrossRef]
7. Wan, H.; Liu, Z.; Liu, G.; Yi, S.; Yan, P.; Deng, H.; Hu, W.; Gao, F. Unraveling TM Migration Mechanisms in LiNi$_{1/3}$Mn$_{1/3}$Co$_{1/3}$O$_2$ by Modeling and Experimental Studies. *Nano Lett.* **2021**, *21*, 6875–6881. [CrossRef]

11 of 11

8. Wang, H.; Yang, G.; Lai, F.; Chu, Y.; Zhang, X.; Ma, Z.; Li, Q. Ultrathin Al_2O_3 Layer Modified $LiNi_{0.6}Co_{0.2}Mn_{0.2}O_2$ with Al-Doping for High Performance Lithium Ion Batteries. *Ionics* **2020**, *26*, 2147–2156. [CrossRef]
9. David, L.; Dahlberg, K.; Mohanty, D.; Ruther, R.E.; Huq, A.; Chi, M.; An, S.J.; Mao, C.; King, D.M.; Stevenson, L.; et al. Unveiling the Role of Al_2O_3 in Preventing Surface Reconstruction During High-Voltage Cycling of Lithium-Ion Batteries. *ACS Appl. Energy Mater.* **2019**, *2*, 1308–1313. [CrossRef]
10. Liu, X.; Wang, S.; Wang, L.; Wang, K.; Wu, X.; Zhou, P.; Miao, Z.; Zhou, J.; Zhao, Y.; Zhuo, S. Stabilizing the High-Voltage Cycle Performance of $LiNi_{0.8}Co_{0.1}Mn_{0.1}O_2$ Cathode Material by Mg Doping. *J. Power Sources* **2019**, *438*, 227017. [CrossRef]
11. Yue, P.; Wang, Z.; Guo, H.; Xiong, X.; Li, X. A Low Temperature Fluorine Substitution on the Electrochemical Performance of Layered $LiNi_{0.8}Co_{0.1}Mn_{0.1}O_{2-z}F_z$ Cathode Materials. *Electrochim. Acta* **2013**, *92*, 1–8. [CrossRef]
12. Zhao, W.; Wang, K.; Dubey, R.; Ren, F.; Brack, E.; Becker, M.; Grissa, R.; Seidl, L.; Pagani, F.; Egorov, K.; et al. Extending the High-Voltage Operation of Graphite/NCM811 Cells by Constructing a Robust Electrode/Electrolyte Interphase Layer. *Mater. Today Energy* **2023**, *34*, 101301. [CrossRef]
13. Zhao, W.; Zheng, G.; Lin, M.; Zhao, W.; Li, D.; Guan, X.; Ji, Y.; Ortiz, G.F.; Yang, Y. Toward a Stable Solid-Electrolyte-Interfaces on Nickel-Rich Cathodes: $LiPO_2F_2$ Salt-Type Additive and Its Working Mechanism for $LiNi_{0.5}Mn_{0.25}Co_{0.25}O_2$ Cathodes. *J. Power Sources* **2018**, *380*, 149–157. [CrossRef]
14. Li, J.; Yang, X.; Guan, X.; Guo, R.; Che, Y.; Lan, J.; Xing, L.; Xu, M.; Fan, W.; Li, W. Efficiently Suppressing Oxygen Evolution in High Voltage Graphite/NCM Pouch Cell with Tributyl Borate as Electrolyte Additive. *Electrochim. Acta* **2020**, *354*, 136722. [CrossRef]
15. Zhang, Z.; Liu, F.; Huang, Z.; Yi, M.; Fan, X.; Bai, M.; Hong, B.; Zhang, Z.; Li, J.; Lai, Y. Improving Interfacial Stability of Ultrahigh-Voltage Lithium Metal Batteries with Single-Crystal Ni-Rich Cathode via a Multifunctional Additive Strategy. *J. Colloid Interface Sci.* **2022**, *608*, 1471–1480. [CrossRef] [PubMed]
16. Beltrop, K.; Klein, S.; Nölle, R.; Wilken, A.; Lee, J.J.; Köster, T.K.-J.; Reiter, J.; Tao, L.; Liang, C.; Winter, M.; et al. Triphenylphosphine Oxide as Highly Effective Electrolyte Additive for Graphite/NMC811 Lithium Ion Cells. *Chem. Mater.* **2018**, *30*, 2726–2741. [CrossRef]
17. Su, C.-C.; He, M.; Peebles, C.; Zeng, L.; Tornheim, A.; Liao, C.; Zhang, L.; Wang, J.; Wang, Y.; Zhang, Z. Functionality Selection Principle for High Voltage Lithium-Ion Battery Electrolyte Additives. *ACS Appl. Mater. Interfaces* **2017**, *9*, 30686–30695. [CrossRef]
18. Dong, Q.; Guo, F.; Cheng, Z.; Mao, Y.; Huang, R.; Li, F.; Dong, H.; Zhang, Q.; Li, W.; Chen, H.; et al. Insights into the Dual Role of Lithium Difluoro(Oxalato)Borate Additive in Improving the Electrochemical Performance of NMC811||Graphite Cells. *ACS Appl. Energy Mater.* **2020**, *3*, 695–704. [CrossRef]
19. Shkrob, I.A.; Zhu, Y.; Marin, T.W.; Abraham, D.P. Mechanistic Insight into the Protective Action of Bis(Oxalato)Borate and Difluoro(Oxalate)Borate Anions in Li-Ion Batteries. *J. Phys. Chem. C* **2013**, *117*, 23750–23756. [CrossRef]
20. Li, Y.; Cheng, B.; Jiao, F.; Wu, K. The Roles and Working Mechanism of Salt-Type Additives on the Performance of High-Voltage Lithium-Ion Batteries. *ACS Appl. Mater. Interfaces* **2020**, *12*, 16298–16307. [CrossRef]
21. Chen, Y.; Zhao, W.; Zhang, Q.; Yang, G.; Zheng, J.; Tang, W.; Xu, Q.; Lai, C.; Yang, J.; Peng, C. Armoring $LiNi_{1/3}Co_{1/3}Mn_{1/3}O_2$ Cathode with Reliable Fluorinated Organic–Inorganic Hybrid Interphase Layer toward Durable High Rate Battery. *Adv. Funct. Mater.* **2020**, *30*, 2000396. [CrossRef]
22. Ma, L.; Ellis, L.; Glazier, S.L.; Ma, X.; Dahn, J.R. Combinations of $LiPO_2F_2$ and Other Electrolyte Additives in $Li[Ni_{0.5}Mn_{0.3}Co_{0.2}]O_2$/Graphite Pouch Cells. *J. Electrochem. Soc.* **2018**, *165*, A1718–A1724. [CrossRef]
23. Gao, H.; Maglia, F.; Lamp, P.; Amine, K.; Chen, Z. Mechanistic Study of Electrolyte Additives to Stabilize High-Voltage Cathode–Electrolyte Interface in Lithium-Ion Batteries. *ACS Appl. Mater. Interfaces* **2017**, *9*, 44542–44549. [CrossRef]
24. Li, X.; Zheng, J.; Ren, X.; Engelhard, M.H.; Zhao, W.; Li, Q.; Zhang, J.; Xu, W. Dendrite-Free and Performance-Enhanced Lithium Metal Batteries through Optimizing Solvent Compositions and Adding Combinational Additives. *Adv. Energy Mater.* **2018**, *8*, 1703022. [CrossRef]
25. Li, X.; Zheng, J.; Engelhard, M.H.; Mei, D.; Li, Q.; Jiao, S.; Liu, N.; Zhao, W.; Zhang, J.-G.; Xu, W. Effects of Imide–Orthoborate Dual-Salt Mixtures in Organic Carbonate Electrolytes on the Stability of Lithium Metal Batteries. *ACS Appl. Mater. Interfaces* **2018**, *10*, 2469–2479. [CrossRef] [PubMed]
26. Zhao, W.; Zou, L.; Zheng, J.; Jia, H.; Song, J.; Engelhard, M.H.; Wang, C.; Xu, W.; Yang, Y.; Zhang, J. Simultaneous Stabilization of $LiNi_{0.76}Mn_{0.14}Co_{0.10}O_2$ Cathode and Lithium Metal Anode by Lithium Bis(Oxalato)Borate as Additive. *ChemSusChem* **2018**, *11*, 2211–2220. [CrossRef]
27. Zhao, W.; Zheng, J.; Zou, L.; Jia, H.; Liu, B.; Wang, H.; Engelhard, M.H.; Wang, C.; Xu, W.; Yang, Y.; et al. High Voltage Operation of Ni-Rich NMC Cathodes Enabled by Stable Electrode/Electrolyte Interphases. *Adv. Energy Mater.* **2018**, *8*, 1800297. [CrossRef]
28. Zhang, Z.; Yang, J.; Huang, W.; Wang, H.; Zhou, W.; Li, Y.; Li, Y.; Xu, J.; Huang, W.; Chiu, W.; et al. Cathode-Electrolyte Interphase in Lithium Batteries Revealed by Cryogenic Electron Microscopy. *Matter* **2021**, *4*, 302–312. [CrossRef]